

**Branching Ratios for the Reactions of OH with Ethanol Amines used in
Carbon Capture and the Potential Impact on Carcinogen Formation in the
Emission Plume from a Carbon Capture Plant**

L. Onel,^{*a} M.A. Blitz,^{ab} J. Breen,^a A.R. Rickard,^{cd} and P.W. Seakins,^{*ab}

^a *School of Chemistry, University of Leeds, Leeds, LS2 9JT, UK. Email:
chmlo@leeds.ac.uk*

^b *National Centre for Atmospheric Science (NCAS), University of Leeds, Leeds,
LS2 9JT, UK*

^c *Wolfson Atmospheric Chemistry Laboratories, Department of Chemistry,
University of York, York, YO10 5DD, UK*

^d *National Centre for Atmospheric Science (NCAS), University of York, York,
YO10 5DD, UK*

Supplementary information

The notation of the quantities and the used abbreviations are the same as in main text.

1. OH + DMEA reaction in the absence/presence of O₂

Figure S1 shows the clear reduction in the observed bimolecular rate coefficient in the presence of excess oxygen.

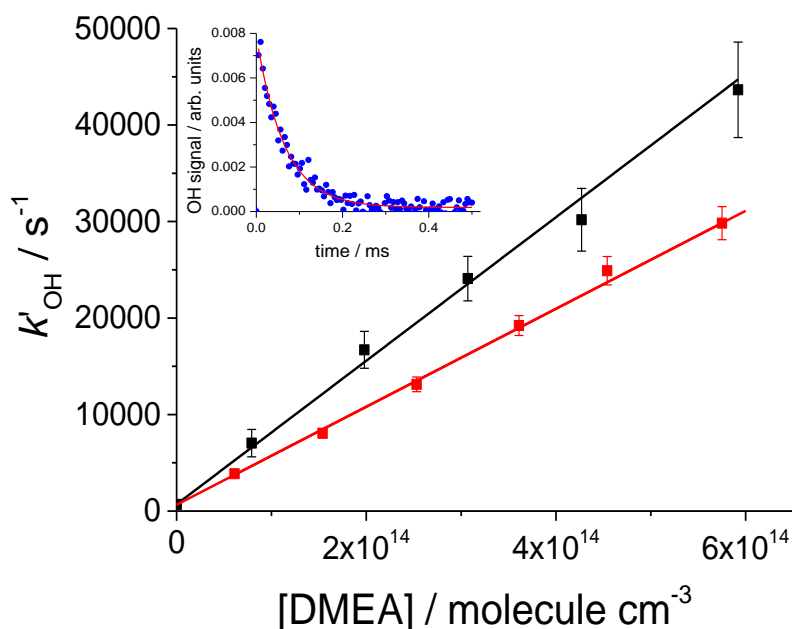


Fig. S1 - Bimolecular plots for DMEA in the absence of O₂, $(7.44 \pm 0.44) \times 10^{-11} \text{ cm}^3 \text{ molecule}^{-1} \text{ s}^{-1}$, black squares and line, and in the presence of O₂, $(5.07 \pm 0.26) \times 10^{-11} \text{ cm}^3 \text{ molecule}^{-1} \text{ s}^{-1}$, red circles and line. Both studies carried out at 298 K and a total pressure of 14 Torr of 100 % N₂ or 90% N₂ + 10% O₂. A typical OH fluorescence decay trace and fit to equation E1 in main text is shown in the inset.

2. Stern-Volmer plots for OH yield from OH + d₄-DMEA reactions with O₂

Fig. S2 shows $1/\Phi_{\text{OH}}$ vs [M] for d₄-DMEA + OH/O₂ system at 298 K. The result is similar to that for nondeuterated DMEA at room temperature. The Stern-Volmer parameters obtained by the unconstrained fits have overlapping error bars and the gradients of the fits at 298 K in Fig. S2 and Fig. 3 are close to each other (Table S1). The result suggests that, in both systems DMEA/O₂ and d₄-DMEA/O₂, the OH regeneration is described by the same chemistry scheme (reactions R8-R10 in main text).

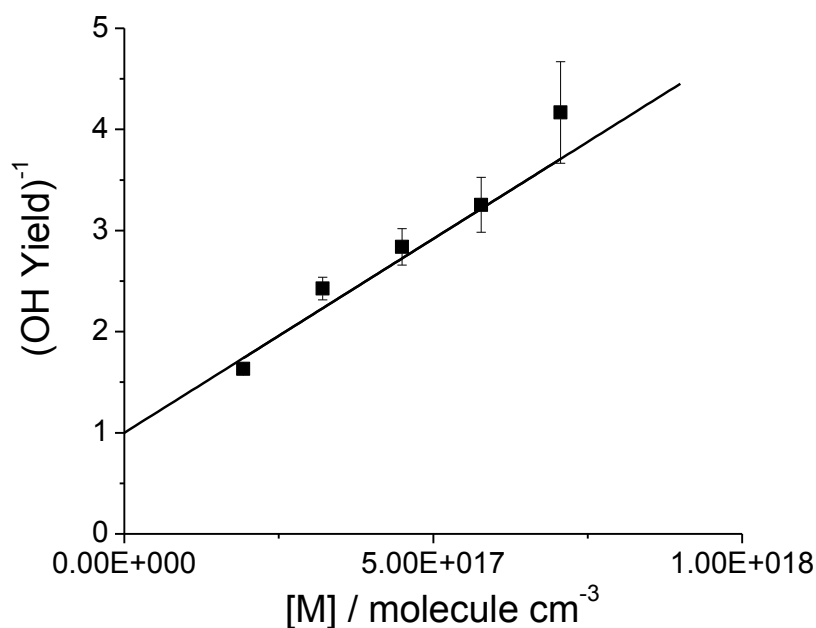


Fig. S2 - Stern-Volmer plots for OH yield from d_4 -DMEA + OH/O₂ system at 298 K, black squares and line. The fits are constrained through unity intercept.

Table S1 Stern-Volmer parameters for the OH + DMEA/ d_4 -DMEA reactions with O₂ at 298 K.

T (K)	Unconstrained intercept				Intercept constrained to unity	
	Intercept ^a		Gradient ^a / cm ³ molecule ⁻¹ / 10 ⁻¹⁸		Gradient ^a / cm ³ molecule ⁻¹ / 10 ⁻¹⁸	
	DMEA	d_4 -DMEA	DMEA	d_4 -DMEA	DMEA	d_4 -DMEA
298	0.88 ± 0.13	0.73 ± 0.12	5.31 ± 0.66	4.81 ± 0.44	4.79 ± 0.26	3.84 ± 0.17

^a Obtained by weighting the linear fit by the error bars, 2σ , of reciprocal of OH yield

3. OH/OD + d_4 -DMEA reaction with O_2 . Determination of the dominant abstraction site of DMEA in reaction with OH

The unconstrained Stern-Volmer plots for the OH + DMEA/ O_2 and OH + d_4 -DMEA/ O_2 systems have intercept values which are consistent with unity OH yield at zero pressure (Table S1), i.e. there is not another route leading to a set of products excluding OH. This result shows that OH abstraction occurs at the C-H sites next to amine group. In order to identify which one from the two α positions (CH_2 or CH_3) is the dominant abstraction site we monitored the OH and OD radicals obtained by the photolysis at 248 nm of d_4 -DMEA in the presence of oxygen (Fig. S3).

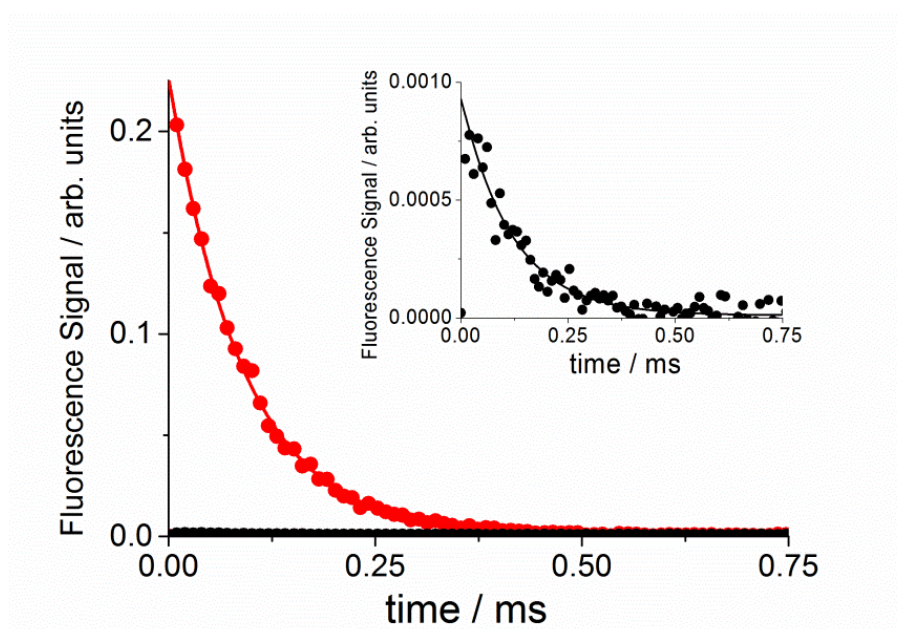
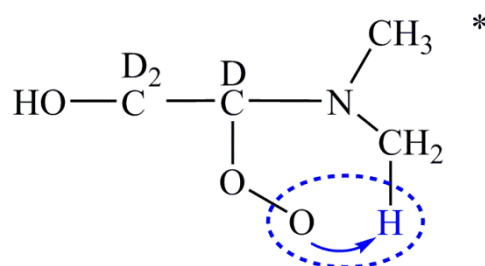


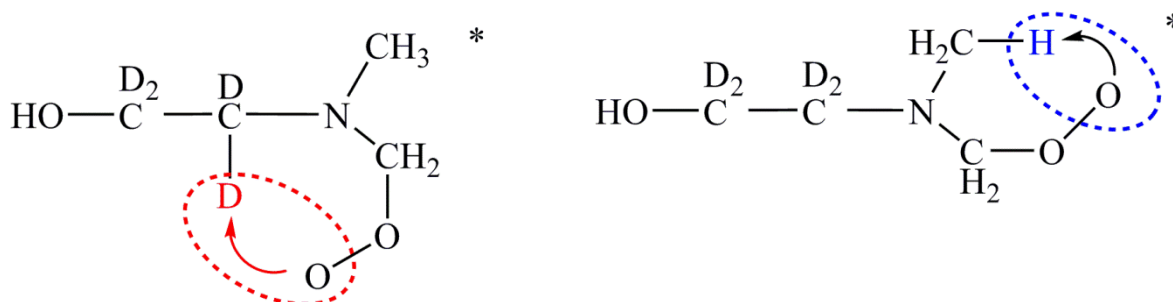
Fig. S3 Parallel measurements of OH (red circles and line) and OD (black circles and line) kinetic decays for OH/OD + $(CH_3)_2N(CD_2)_2OH$ reaction at 298K and a total pressure of 15 Torr of 80% N_2 + 20% O_2 . The OD signal was divided by the response factor for OD over OH of 1.86.¹ The inset shows the OD signal magnified.

In Fig. S3 the OH signal at time zero is ~250 times higher than the adjusted OD signal at time zero. The domination of the initial hydroxyl signal by OH following the photolysis of d_4 -DMEA suggests that photolysis primarily occurs at the α CD_2 site. The generated carbon-

centred radical reacts with O₂ to form an activated peroxy radical which decomposes to produce OH as illustrated below:



A growth in the OD signal might be expected if OH abstracted from the CH₃ groups as, in this case, the internal abstraction in the activated peroxy species might occur from both CD₂ and CH₃ groups as shown schematically below:

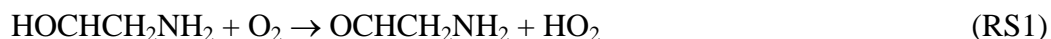


However, there is no growth in the OD signal (inset of Figure S3), hence the initial abstraction occurs from α methylene group.

4. OH + MEA/MMEA/MeOEA reactions in the presence of O₂/NO

4.1. Determination of the dominant abstraction site of MEA in reaction with OH using the OH + MeOEA/O₂ system

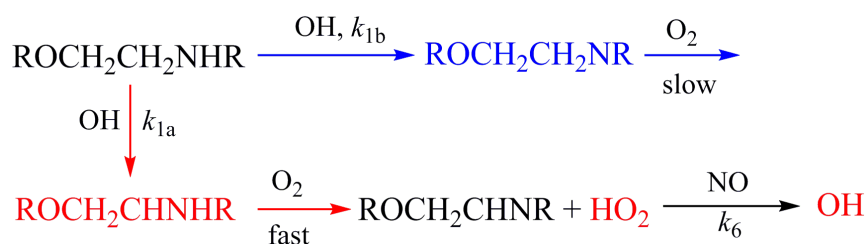
On the millisecond scale of the OH + MEA/O₂/NO experiments, HO₂ is generated through reaction R5 of the α carbon-centred radical produced *via* R1a (main text) and/or through reaction RS1 of the β carbon-centred radical generated *via* R1c. Reaction RS1 is similar to the α -hydroxyalkyl + O₂ reactions.



In order to determine which one from the two C-H positions in MEA is the dominant abstraction site in reaction with OH we determined if the HO₂ yield is altered by using MeOEA (CH₃OCH₂CH₂NH₂) instead of MEA (HOCH₂CH₂NH₂) as, in the OH + MeOEA/O₂ system, initial abstraction at β position cannot result in formation of HO₂. The resultant Φ_{HO₂, MeOEA} = 0.69 ± 0.09 at 20 Torr and Φ_{HO₂, MeOEA} = 0.68 ± 0.06 at 40 Torr are within the error limits of Φ_{HO₂, MEA} = 0.62 ± 0.06 in the range 20 – 150 Torr (Table 2 in main text). Therefore, the results strongly suggest the dominant H-abstraction site of MEA is in the α position.

4.2. Determination of the HO₂ yield

In the presence of NO reaction R6 regenerates OH in the OH + MEA/MMEA/MeOEA/O₂ systems and the OH decays are biexponential in nature (see the example shown in the inset of Fig. S4). The method for assign HO₂ yield was described previously¹ and is illustrated schematically:



The biexponential OH decays were fitted to the solution of the rate equations for reactions R1a, R1b and R6 to determine the pseudo-first-order rate coefficients k'_{1a} and k'_{1b} and k'_6 .¹

The determined parameters were used to assign the HO₂ yield, Φ_{HO₂} and hence r_{1a} and r_{1b} :

$$\Phi_{\text{HO}_2} = r_{1a} = \frac{k'_{1a}}{k'_1} = 1 - \frac{k'_{1b}}{k'_1} = 1 - r_{1b} \quad (\text{equation S1})$$

The parameter k'_6 allowed the determination of the bimolecular rate coefficient of the NO reaction with HO₂ as the gradient of the linear fit of k'_6 vs [NO] (see Fig. S4 as an example). The gradient of the bimolecular plot shown in Fig. S4, $(9.95 \pm 0.35) \times 10^{-12} \text{ cm}^3 \text{ molecule}^{-1} \text{ s}^{-1}$, is consistent with the recommendation of Atkinson et al., $(8.8 \pm 2.4) \times 10^{-12} \text{ cm}^3 \text{ molecule}^{-1} \text{ s}^{-1}$,² and with our previous determinations: $(1.11 \pm 0.14) \times 10^{-11} \text{ cm}^3 \text{ molecule}^{-1} \text{ s}^{-1}$ for OH + methylamine/NO/O₂ system, $(1.13 \pm 0.11) \times 10^{-11}$ for OH + methanol/NO/O₂ system and $(1.05 \pm 0.12) \times 10^{-11} \text{ cm}^3 \text{ molecule}^{-1} \text{ s}^{-1}$ for OH + ethanol/NO/O₂ system.¹

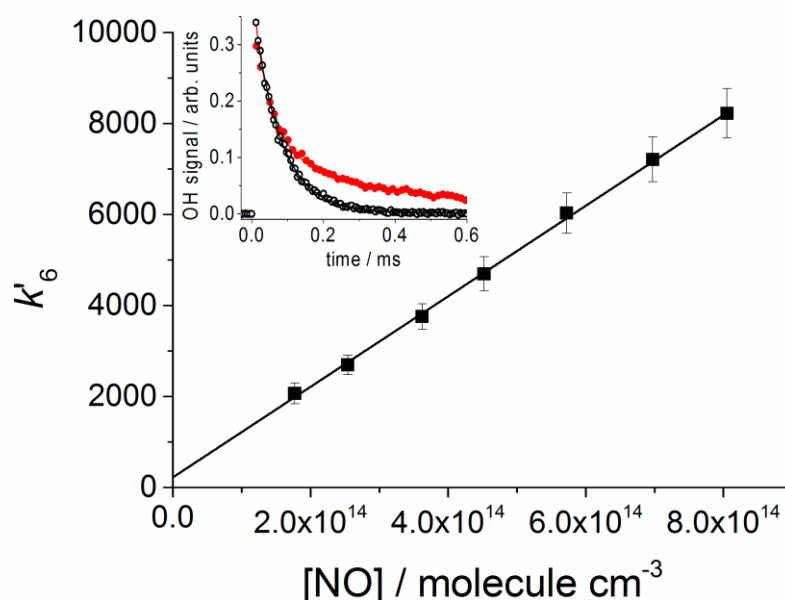


Fig. S4 Bimolecular plot for the reaction of NO with HO₂ generated in OH + MEA/O₂ system. The inset shows the single exponential OH decay in the absence of NO (black squares) and the biexponential decay in the presence of $6.97 \times 10^{14} \text{ molecule cm}^{-3}$ NO (red circles). Experiments performed at 298 K and a total pressure of 20 Torr of 91% N₂ + 9% O₂.

At 248 nm amines photolyse to form H atoms. The subsequent chemistry of H atoms was found to produce a small additional OH signal in the OH + DMA/NO/O₂ and OH + PZ/NO/O₂ systems.^{1,3} However, separate studies showed that the 248 nm cross sections for H atom formation, $\sigma_{248\text{nm,H}}$, of MEA and MMEA are at least one order of magnitude smaller

than $\sigma_{248\text{nm,H}}$ of DMA (10^{-20} cm² molecule⁻¹ orders of magnitude), and at least two orders of magnitude smaller compared to $\sigma_{248\text{nm,H}}$ of PZ (10^{-19} cm² molecule⁻¹ orders of magnitude).⁴ Therefore, the photolytic generation of H atoms was negligible in our experiments and did not affect the results obtained for the OH + MEA/MMEA reactions in the presence of NO/O₂.

5. Structure Activity Relationship (SAR) calculations

Table S2. Room temperature rate coefficients and branching ratios in the reaction of OH with MEA and MMEA determined in this work and calculated using SARs

	Rate coefficients		Branching ratios			
	10 ⁻¹¹ cm ³ molecule ⁻¹ s ⁻¹		Calculated ^b			
	<i>k</i> _{OH}	<i>k</i> _{OH} ^b	<i>r</i> _{αC-H}	<i>r</i> _{βC-H}	<i>r</i> _{N-H / N-attack} ^c	<i>r</i> _{N-CH3}
MEA	7.61 ± 0.76 ⁵	4.04	0.45	0.08	0.47	-
MMEA	8.26 ± 0.82 ^a	8.45	0.21	0.04	0.74	0.01
DMEA	7.29 ± 0.72 ^a	6.95	0.26	0.05	0.66	0.03
			Determined experimentally			
MEA			0.62 ± 0.06		0.38 ± 0.06	
MMEA			0.48 ± 0.03		0.52 ± 0.06	
DMEA			~1.00		-	

^a This work

^b SAR calculations.⁶⁻⁸ OH rate coefficients and branching ratios were calculated using a combination of the following parameters: group rate coefficients for H atom abstraction from C-H bonds and -OH groups (*k*_{prim}, *k*_{sec}, *k*_{tert} and *k*_{OH}) and substituent group factors (*F*(*X*)) are taken from Ziemann and Atkinson.⁶ The SAR parameters for abstraction at an N-H site, *k*_{RNH2} (MEA) and *k*_{R2NH} (MMEA), and for the OH attack at the nitrogen atom, *k*_{R3N} (DMEA), along with the *F*(*X*) values for groups -NH₂, >NH and -N< are taken from Nielsen et al.⁷

^c N-attack results in an initial addition of OH through H-bonding to the nitrogen lone-pair, forming a stable pre-reaction adduct. H-abstraction within the pre-reaction adduct then leads to H₂O and a radical species. Caution is taken when using hydrogen abstraction SARs for amines for reasons given in Nielsen et al.⁷ The formation of pre-reaction OH-amine adducts in which the OH radical is H-bonded to the nitrogen lone-pair results in a negative Arrhenius activation energy, and low energy barrier or barriers to reaction below the energy of reactants.

6. Master Equation Solver for Multi Energy well Reactions (MESMER) calculations

The yield of HO₂ radical in HOCH₂CHNH₂ + O₂ reaction, Γ_{HO_2} , has been calculated in the range of 20 – 150 Torr using the experimental branching ratios r_{1a} for MEA + OH reaction (Table 2 in main text). The HO₂ yield at 20 Torr was assumed equal to unity on average, $\bar{\Gamma}_{\text{HO}_2(20\text{Torr})} = 1$, as in our previous MESMER study of the O₂ reactions with RCHNHR radicals.¹ This assumption was also supported by the experimental finding that the HO₂ yield in the MEA + OH reaction is practically unchanged over 20 – 150 Torr. Γ_{HO_2} at 60 and 150 Torr was determined as follows:

$$\Gamma_{\text{HO}_2(p)} = r_{(1a,p)} / \bar{r}_{(1a,20\text{Torr})} \quad (\text{equation S2})$$

where $\bar{r}_{(1a,20\text{Torr})}$ is the mean of the experimental values of r_{1a} at 20 Torr.

G4 potential energy surface calculations⁹ have been used in a master equation fit of Γ_{HO_2} calculated using equation S2. The parameter ΔE_{down} for N₂ was fixed to 270 cm⁻¹ as in our previous calculations for the O₂ + RCHNHR reactions and in very good agreement with various reported values of ΔE_{down} for N₂.¹⁰⁻¹² The energy barrier between peroxy radical and post-reaction imine-HO₂ complex was floated starting from the *ab initio* value, 90.42 kJ mol⁻¹. The fit found a lower transition state energy, 82.18 ± 0.87 kJ mol⁻¹. The level of agreement between the reaction barrier found by fitting and the *ab initio* result is ~8 kJ mol⁻¹; a slightly lower level of agreement between the MESMER result and the *ab initio* value for CH₃CHNH₂ + O₂ reaction of ~6 kJ mol⁻¹ was found previously.¹ We attribute this lower level of agreement to the larger uncertainty in the G4 theory computation of the energy of the transition state for larger HOCH₂CHNH₂ + O₂ system. Typical errors in high level *ab initio* calculations of stable species are of the order of 2 – 4 kJ mol⁻¹; calculations of transition states will have a higher level of uncertainty and so the observed discrepancy of 6 – 8 kJ mol⁻¹

¹ between the fitted values and the calculated energy of the transition state is not unreasonable.

The energy barrier obtained by fitting was used in MESMER numerical simulations to assign $\Gamma_{\text{HO}_2(1 \text{ atm})} = 0.67 \pm 0.18$ (Fig. 4). The error limits for $\Gamma_{\text{HO}_2(1 \text{ atm})}$ reported here were determined assuming a typical error in the energy barrier calculation of $\pm 4 \text{ kJ mol}^{-1}$. Similar atmospheric pressure yields of HO_2 were found for the $\text{CH}_3\text{CHNH}_2 + \text{O}_2$ reaction: 0.50 ± 0.18^1 and ~ 0.60 .¹⁰

7. Atmospheric modelling

7.1. MEA chemistry scheme

Table S3. MEA (RCH_2NH_2 , where $\text{R} = \text{HOCH}_2$) oxidation reactions and phase transfer processes incorporated in the atmospheric model

Reaction	Rate coefficient / $\text{cm}^3 \text{ molecule}^{-1} \text{ s}^{-1}$ or s^{-1}	Reference
Gas phase reactions		
$\text{RCH}_2\text{NH}_2 + \text{OH} \rightarrow \text{RCHNH}_2$	$0.62 \times k_{\text{OH}}^a$	This work and Onel et al. ⁵
$\text{RCH}_2\text{NH}_2 + \text{OH} \rightarrow \text{RCH}_2\text{NH}$	$0.38 \times k_{\text{OH}}^a$	This work and Onel et al. ⁵
$\text{RCHNH}_2 + \text{O}_2 \rightarrow \text{RCHNH} + \text{HO}_2$	$0.67 \times k_{\text{O}_2}^b$	This work and Rissanen et al. ¹⁰
$\text{RCHNH}_2 + \text{O}_2 \rightarrow \text{RCH}(\text{O}_2)\text{NH}_2$	$0.33 \times k_{\text{O}_2}^b$	This work and Rissanen et al. ¹⁰

$\text{RCH(O}_2\text{)NH}_2 + \text{HO}_2 \rightarrow \text{RCH(O}_2\text{H)NH}_2$ + O_2	5.7×10^{-12}	Considered equal to the rate coefficient for the $\text{CH}_3\text{O}_2 + \text{HO}_2$ reaction ¹³
$\text{RCH(O}_2\text{)NH}_2 + \text{NO} \rightarrow \text{RCH(O)NH}_2 + \text{NO}_2$	8.0×10^{-12}	Considered equal to the rate coefficient for the $\text{CH}_3\text{O}_2 + \text{NO}$ reaction ¹³
$\text{RCH(O)NH}_2 + \text{O}_2 \rightarrow \text{RCONH}_2 + \text{HO}_2$	2.4×10^{-15}	Karl et al. ¹⁴
$\text{RCH(O)NH}_2 \rightarrow \text{HCONH}_2 + \text{HCHO} + \text{HO}_2$	2.0×10^5	Karl et al. ¹⁴
$\text{HCONH}_2 + \text{OH} \rightarrow \text{HNCO} + \text{HO}_2$	4.5×10^{-12}	Estimated ^c
$\text{RCONH}_2 + \text{OH} \rightarrow \text{HCOCONH}_2 + \text{HO}_2$	4.6×10^{-12}	Karl et al. ¹⁴
$\text{RCH}_2\text{NH} + \text{NO}_2 \rightarrow \text{RCH}_2\text{NHNO}_2$	$k_{\text{NO}_2}^d$	Lazarou et al. ¹⁵
$\text{RCH}_2\text{NH} + \text{NO}_2 \rightarrow \text{RCHNH} + \text{HONO}$	$0.22 \times k_{\text{NO}_2}^d$	Lindley et al. ¹⁶ and Lazarou et al. ¹⁵
$\text{RCH}_2\text{NH} + \text{NO} \rightarrow \text{RCH}_2\text{NHNO}$	k_{NO}^e	Lazarou et al. ¹⁵
$\text{RCH}_2\text{NH} + \text{O}_2 \rightarrow \text{RCHNH} + \text{HO}_2$	$3.9 \times 10^{-7} \times k_{\text{NO}_2}^d$	Lindley et al. ¹⁶ and Lazarou et al. ¹⁵
$\text{RCH}_2\text{NHNO}_2 + \text{OH} \rightarrow \text{RCONHNO}_2$	3.5×10^{-12f}	Maguta et al. ¹⁷
$\text{RCH}_2\text{NHNO} \rightarrow \text{RCH}_2\text{NH} + \text{NO}$	$0.34 \times j_{\text{NO}_2}$	Nielsen et al. ⁷

Phase transfer and aqueous reactions with OH		
$\text{RCH}_2\text{NH}_2 \rightarrow (\text{RCH}_2\text{NH}_2)_{\text{aq}}$	-	This work ^g
$(\text{RCH}_2\text{NH}_2)_{\text{aq}} \rightarrow \text{RCH}_2\text{NH}_2$	-	This work ^h
$(\text{RCH}_2\text{NH}_2)_{\text{aq}} + (\text{OH})_{\text{aq}} \rightarrow (\text{P1})_{\text{aq}}$	$k_{\text{aq}}^{\text{MEA}} \times [\text{OH}]_{\text{aq}}^{\text{av}}$	<i>i</i>
$\text{RCH}_2\text{NHNO}_2 \rightarrow (\text{RCH}_2\text{NHNO}_2)_{\text{aq}}$	-	This work ^g
$(\text{RCH}_2\text{NHNO}_2)_{\text{aq}} \rightarrow \text{RCH}_2\text{NHNO}_2$	-	This work ^h
$(\text{RCH}_2\text{NHNO}_2)_{\text{aq}} + (\text{OH})_{\text{aq}} \rightarrow (\text{P2})_{\text{aq}}$	$k_{\text{aq}}^{\text{RNNNO}_2} \times [\text{OH}]_{\text{aq}}^{\text{av}}$	<i>i</i>
$\text{RCH}_2\text{NHNO} \rightarrow (\text{RCH}_2\text{NHNO})_{\text{aq}}$	-	This work ^g
$(\text{RCH}_2\text{NHNO})_{\text{aq}} \rightarrow \text{RCH}_2\text{NHNO}$	-	This work ^h
$(\text{RCH}_2\text{NHNO})_{\text{aq}} + (\text{OH})_{\text{aq}} \rightarrow (\text{P3})_{\text{aq}}$	$k_{\text{aq}}^{\text{RNNNO}} \times [\text{OH}]_{\text{aq}}^{\text{av}}$	<i>i</i>

^a $k_{\text{OH}} = 7.6 \times 10^{-11} \text{ cm}^3 \text{ molecule}^{-1} \text{ s}^{-1}$ ⁵

^b $k_{\text{O}_2} = 5 \times 10^{-11} \text{ cm}^3 \text{ molecule}^{-1} \text{ s}^{-1}$. Estimated using the profile of the rate coefficient for the reaction of O₂ with CH₂NH₂ vs pressure reported for N₂ by Rissanen et al.¹⁰

^c Calculated as ten times lower than the rate coefficient for the HCONH₂ + Cl reaction based on the kinetic data reviewed by Nielsen et al. showing that the rate coefficients for the amide + OH reactions are one order of magnitude lower than the rate coefficients for the amide + Cl reactions.⁷

^d $k_{\text{NO}_2} = 3.2 \times 10^{-13} \text{ cm}^3 \text{ molecule}^{-1} \text{ s}^{-1}$. Determined experimentally for the (CH₃)₂NH + NO₂ → (CH₃)₂NNO₂ reaction by Lazarou et al.¹⁵

^e $k_{\text{NO}} = 8.5 \times 10^{-14} \text{ cm}^3 \text{ molecule}^{-1} \text{ s}^{-1}$. Determined experimentally for the (CH₃)₂NH + NO → (CH₃)₂NNO reaction by Lazarou et al.¹⁵

^f Equal to the rate coefficient for the OH + (CH₃)₂NNO₂ reaction¹⁷

^g Calculated using equation E3 in main text.

^h Calculated using equation E4 in main text.

ⁱ $k_{\text{aq}}^{\text{MEA}} = 3 \times 10^8 \text{ M}^{-1} \text{ s}^{-1}$, $k_{\text{aq}}^{\text{RNNNO}_2} = 5.4 \times 10^8 \text{ M}^{-1} \text{ s}^{-1}$ as measured for the (CH₃)₂NNO₂ + OH reaction in water by Mezyk et al.¹⁸ and $k_{\text{aq}}^{\text{RNNNO}}$ is equal to the mean of the measurements of Landsman et al.,¹⁹ Wink et al.²⁰ and Lee et al.²¹ for the (CH₃)₂NNO + OH reaction in water, $4.0 \times 10^8 \text{ M}^{-1} \text{ s}^{-1}$. $[\text{OH}]_{\text{aq}}^{\text{av}}$ is the mean concentration of OH in either wet aerosols, 10⁻¹³ M, or cloud droplets, 2 × 10⁻¹² M, in maritime environment.⁷

7.2. Details on the parametrisation of heterogeneous uptake

The uptake coefficients for MEA, R₂N-NO₂ and R₂N-NO are not currently known. In line with the parametrisation of the wet deposition included in the chemical transport model used by Karl et al. to study the environmental impact of carbon capture emissions of MEA,²² we used HNO₃ as a model compound in the parametrisation of heterogeneous uptake. Therefore, in our work the uptake coefficients for MEA, R₂N-NO₂ and R₂N-NO were considered equal to the uptake coefficient for HNO₃, calculated as the mean of the values at room temperature reported by Van Doren et al.,²³ Ponche et al.²⁴ and Schütze and Herrmann,²⁵ $\gamma_{\text{HNO}_3} = 0.07 \pm 0.04$.

The gas diffusion coefficient, D_i^g , in equation E3 (main text) is given by equation S4.

$$D_i^g = \frac{3}{8N_A (d_i^g)^2 \rho_{\text{air}}} \sqrt{\frac{RT M_{\text{air}}}{2\pi} \left(\frac{M_i^g + M_{\text{air}}}{M_i^g} \right)} \quad (\text{equation S4})$$

Here N_A is Avogadro's number, d_i^g is the diameter of the gas molecule i , ρ_{air} is the density of air, R is the gas constant, T is the temperature (K), M_{air} and M_i^g are the molar masses of air and the gas i , respectively. The mean molecular speed \bar{c}_i^g is given by equation S5.

$$\bar{c}_i^g = \sqrt{\frac{8RT}{\pi M_i^g}} \quad (\text{equation S5})$$

7.3. Details on the parametrisation describing the plume dispersion

The plume width at time t , $y(t)$, depends on the width at time zero, $y(0)$, and the horizontal diffusion coefficient, K_y (equation E7 in main text). Due to less turbulent boundary layer at

night than at day, the plume emitted at midnight expands less than the plumes emitted at day.²⁶ For the emission at day time equation E7 was used to fit the time series of the width of the Cumberland power plant plume studied by Ryerson et al.²⁷ (Figure S5) in order to determine the parameter K_y . The plume widths were estimated using profiles of the NO_x , O_3 and SO_2 mixing ratios observed by these authors across the downwind direction. During the fitting, the parameter $y(0)$ was fixed at 2.5 m and 100 m, respectively, while the parameter K_y was floated. In both cases, the fit led to $K_y = 3034 \pm 301 \text{ m}^2 \text{ s}^{-1}$. Therefore, a value of $3034 \text{ m}^2 \text{ s}^{-1}$ was used in numerical simulations.

For the emission at night equation E7 was fit to the total width of the plumes emitted at Oklaunion and Paris power plants vs. transport time to determine K_y . The total width of the plumes, $y(t)$, was calculated using full-width at half maximum, $FWHM(t)$, of the Gaussian fit to SO_2 plumes,²⁶ as it follows²⁸

$$\sigma(t) = \frac{FWHM(t)}{2\sqrt{2\ln 2}} \quad \text{(equation S6)}$$

$$y(t) = 6\sigma(t) \quad \text{(equation S7)}$$

where $\sigma(t)$ is the standard deviation.

The mean of the values of the horizontal diffusion coefficient for the Oklaunion and Parish plumes, $K_y = 573 \pm 102 \text{ m}^2 \text{ s}^{-1}$, was used in the numerical simulations started at midnight.

As the time zero in numerical simulations corresponded to 10 min after emission, for day time emissions $y(0)$ in the simulations equalled $y(10 \text{ min})$ in Fig. S5, 3816 m and for the midnight emission $y(0)$ in simulations equalled $y(10 \text{ min})$ in Fig. S6, 1658 m.

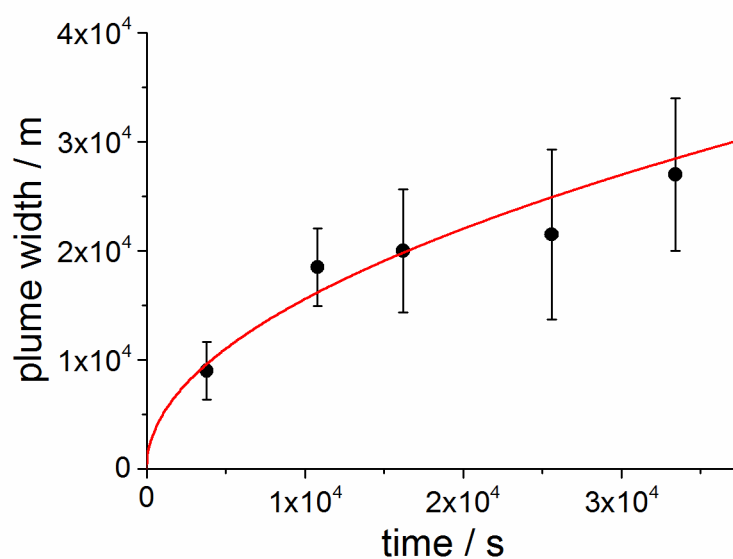


Fig. S5 Fit of the plume width emitted at day from Cumberland power plant²⁷ using equation E7 in main text. The error bars represent standard errors of a series of estimations obtained using the mixing ratio profiles for NO_x , O_3 and SO_2 reported by Ryerson et al.²⁷

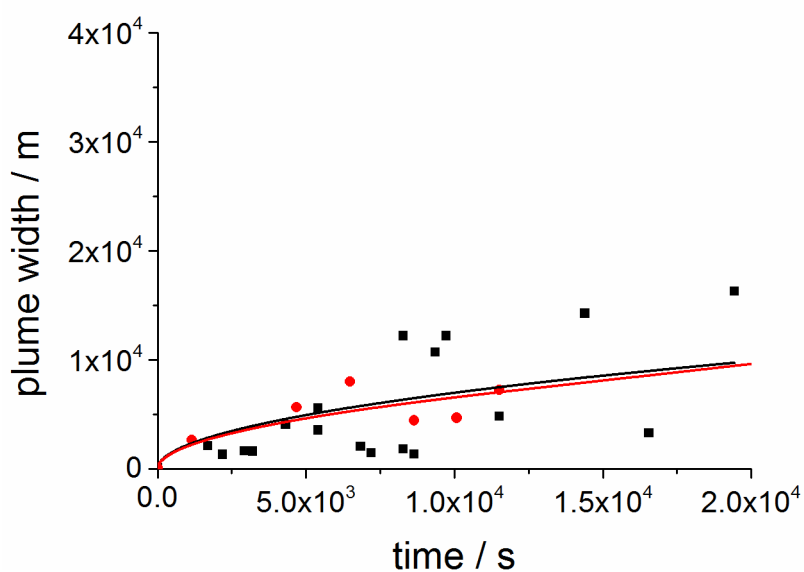


Fig. S6 Fit of the SO_2 plume width emitted at night from Oklaunion (black squares and line) and Parish (red circles and line) power plants.²⁶

7.4. Average diurnal cycles of key species measured for the North-westerly wind sector at Weybourne, September 2002^{29, 30}

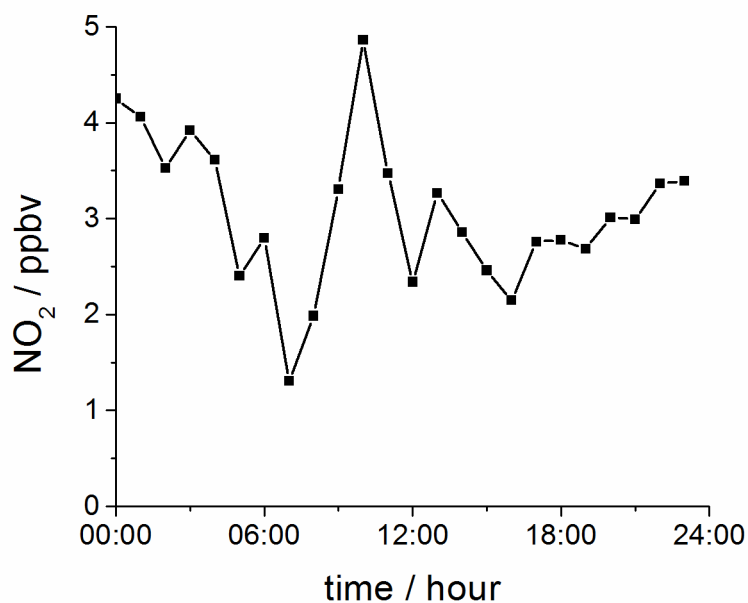


Fig. S7. Hourly averaged diurnal cycle of NO₂. Concentration of NO₂ in parts per billion by volume (ppbv).

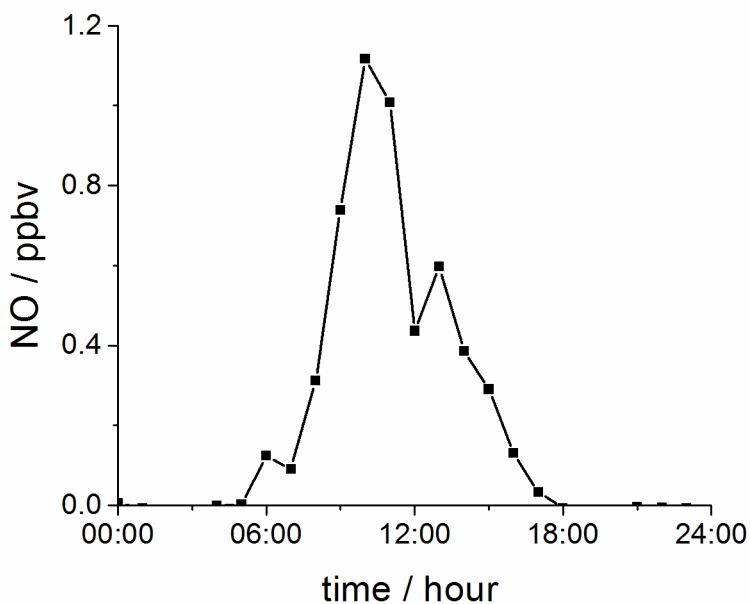


Fig. S8. Hourly averaged diurnal cycle of NO. Concentration of NO in parts per billion by volume (ppbv).

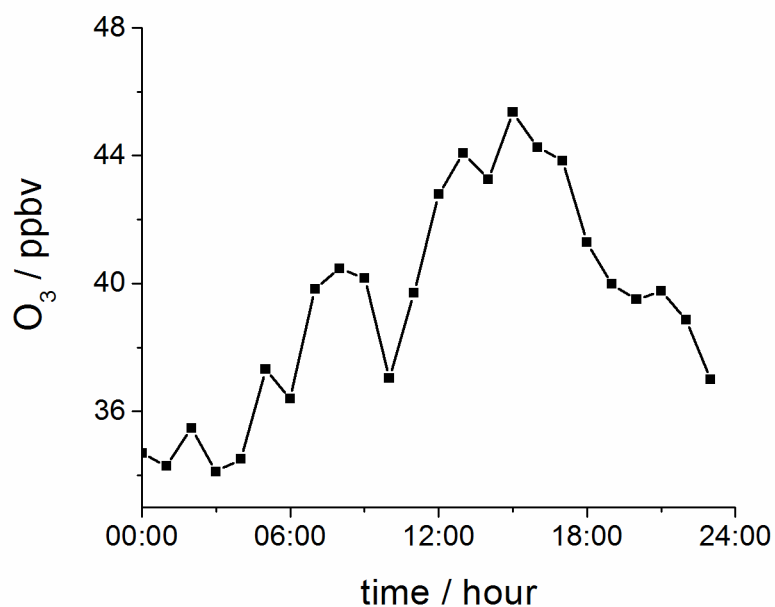


Fig. S9. Hourly averaged diurnal cycle of O₃. Concentration of O₃ in parts per billion by volume (ppbv).

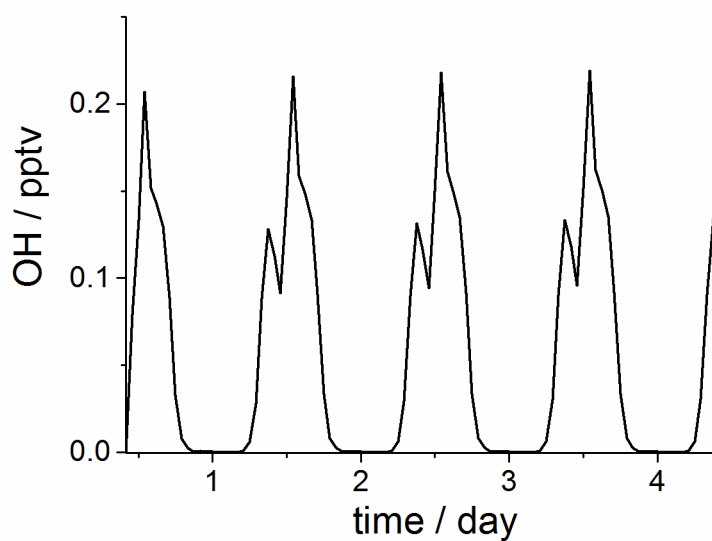


Fig. S10 Diurnal cycle of OH radical generated by running the background model described in the main text for four days. Numerical simulations starts at 10:00.

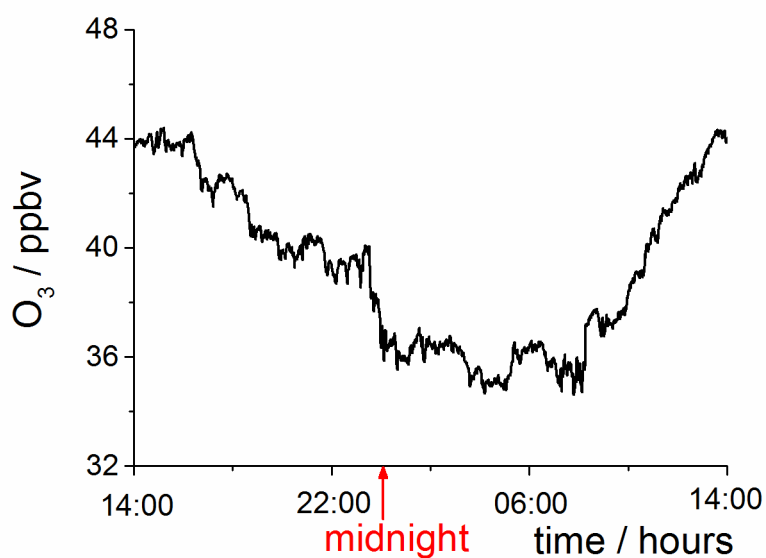


Fig. S11 One minute averaged diurnal cycle of ozone measured at Weybourne from 17 to 29 September 2002 used in the numerical simulations started at 14:00.

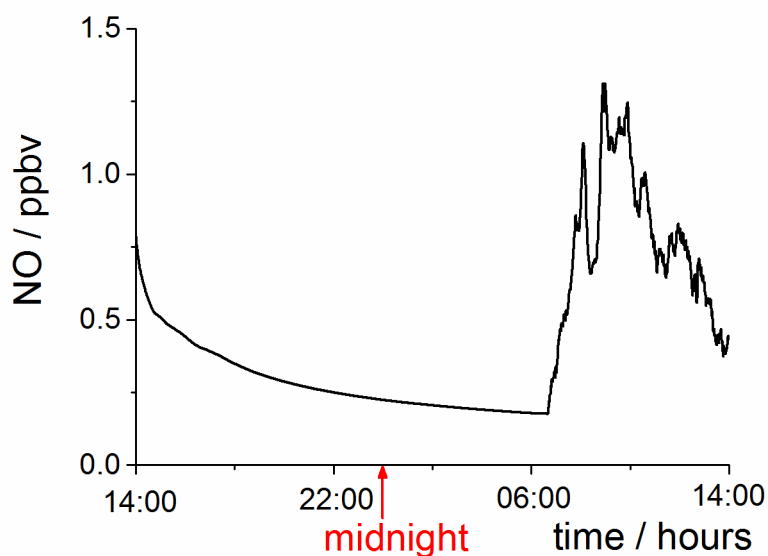


Fig. S12 NO concentration generated by numerical simulations (see main text) for emission at 14:00. Next day after emission, at ~ 07:00 the concentration of NO within the plume equals the ambient concentration of NO, constrained to the one minute averaged diurnal cycle measured at Weybourne from 17 to 29 September 2002.

7.5. Rates of MEA losses for emission at midnight

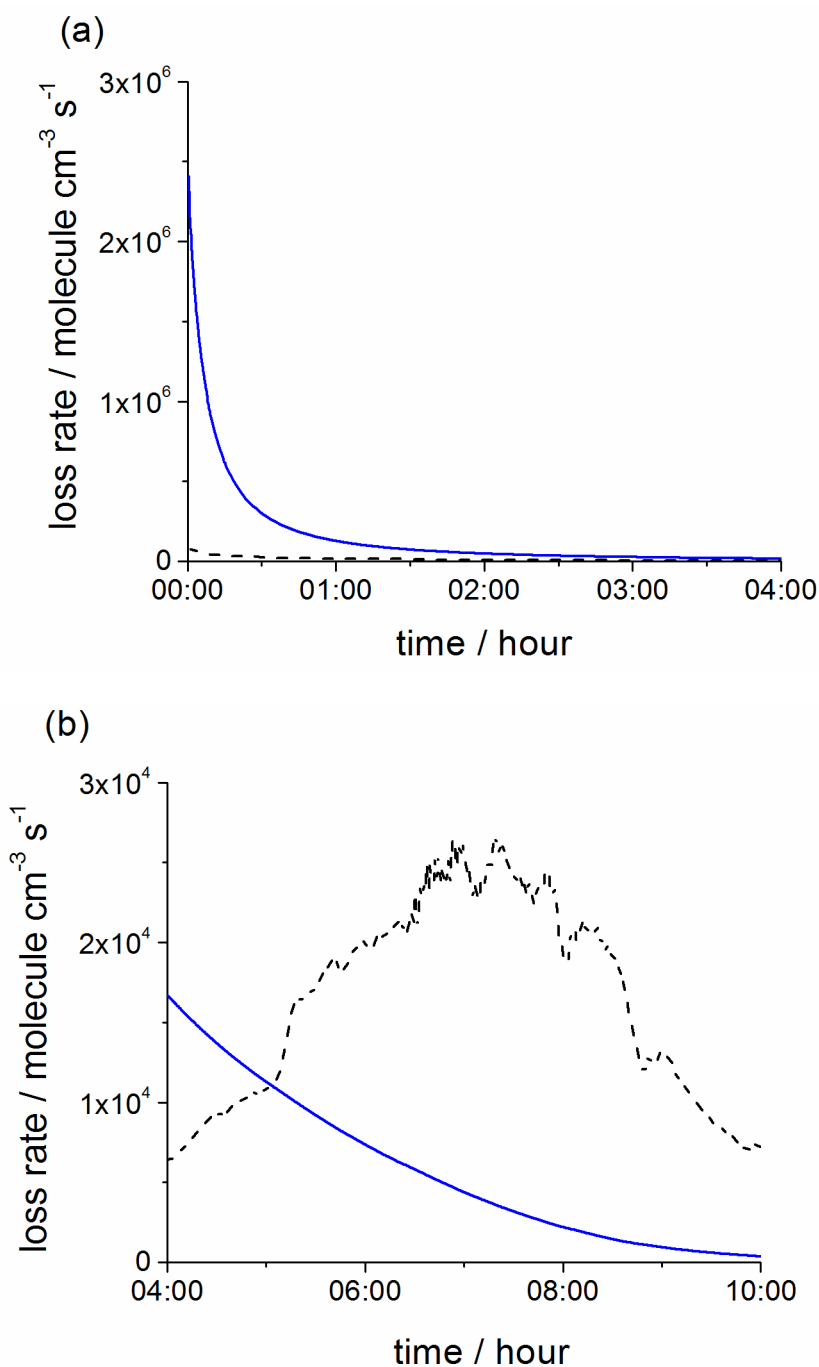


Fig. S13 Loss rates of MEA vs. time after emission from PCCC plant at 00:00 under cloud free conditions: dispersion rate (blue solid line) and rate of the OH + MEA reaction (black dash line): (a) plot over the first four hours after emission; (b) plot over 04:00 – 10:00. Model does not include the $\text{NO}_3 + \text{MEA}$ reaction. With the exception of the first minute, when the uptake rate of MEA is $\sim 10^6 \text{ molecule cm}^{-3} \text{s}^{-1}$, almost no uptake of MEA onto aerosols occurs as Henry's law is practically fulfilled at almost all the simulation times.

1. L. Onel, M. Blitz, M. Dryden, L. Thonger and P. Seakins, *Environmental Science & Technology*, 2014, **48**, 9935-9942.
2. R. Atkinson, D. L. Baulch, R. A. Cox, J. N. Crowley, R. F. Hampson, R. G. Hynes, M. E. Jenkin, M. J. Rossi and J. Troe, *Atmospheric Chemistry and Physics*, 2004, **4**, 1461-1738.
3. L. Onel, M. Dryden, M. A. Blitz and P. W. Seakins, *Environmental Science & Technology Letters*, 2014, **1**, 367-371.
4. L. Onel, M. A. Blitz, M. Dryden and P. W. Seakins.
5. L. Onel, M. A. Blitz and P. W. Seakins, *J. Phys. Chem. Lett.*, 2012, **3**, 853-856.
6. P. J. Ziemann and R. Atkinson, *Chem. Soc. Rev.*, 2012, **41**, 6582-6605.
7. C. J. Nielsen, H. Herrmann and C. Weller, *Chem. Soc. Rev.*, 2012, **41**, 6684-6704.
8. E. S. C. Kwok and R. Atkinson, *Atmos. Environ.*, 1995, **29**, 1685-1695.
9. C. J. Nielsen, personal communication.
10. M. P. Rissanen, A. J. Eskola, T. L. Nguyen, J. R. Barker, J. Liu, J. Liu, E. Halme and R. S. Timonen, *J. Phys. Chem. A*, 2014, **118**, 2176-2186.
11. S. A. Carr, D. R. Glowacki, C.-H. Liang, M. T. Baeza-Romero, M. A. Blitz, M. J. Pilling and P. W. Seakins, *Journal of Physical Chemistry A*, 2011, **115**, 1069-1085.
12. K. W. McKee, M. A. Blitz, P. A. Cleary, D. R. Glowacki, M. J. Pilling, P. W. Seakins and L. Wang, *Journal of Physical Chemistry A*, 2007, **111**, 4043-4055.
13. <http://mcm.leeds.ac.uk/MCM>.
14. M. Karl, C. Dye, N. Schmidbauer, A. Wisthaler, T. Mikoviny, B. D'Anna, M. Muller, E. Borras, E. Clemente, A. Munoz, R. Porras, M. Rodenas, M. Vazquez and T. Brauers, *Atmos. Chem. Phys.*, 2012, **12**, 1881-1901.
15. Y. G. Lazarou, K. G. Kampanis and P. Papagiannakopoulos, *J. Phys. Chem.*, 1994, **98**, 2110-2115.
16. C. R. C. Lindley, J. G. Calvert and J. H. Shaw, *Chemical Physics Letters*, 1979, **67**, 57-62.
17. M. M. Maguta, M. Aursnes, A. J. C. Bunkan, K. Edelen, T. Mikoviny, C. J. Nielsen, Y. Stenstrom, Y. Tang and A. Wisthaler, *J. Phys. Chem. A*, 2014, **118**, 3450-3462.
18. S. P. Mezyk, D. B. Ewing, J. J. Kiddle and K. P. Madden, *J. Phys. Chem. A*, 2006, **110**, 4732-4737.
19. N. A. Landsman, K. L. Swancutt, C. N. Bradford, C. R. Cox, J. J. Kiddle and S. P. Mezyk, *Environ. Sci. Technol.*, 2007, **41**, 5818-5823.
20. D. A. Wink, R. W. Nims, M. F. Desrosiers, P. C. Ford and L. K. Keefer, *Chem. Res. Toxicol.*, 1991, **4**, 510-512.
21. C. Lee, J. Yoon and U. Von Gunten, *Water Res.*, 2007, **41**, 581-590.
22. M. Karl, N. Castell, D. Simpson, S. Solberg, J. Starrfelt, T. Svendby, S. E. Walker and R. F. Wright, *Atmos. Chem. Phys.*, 2014, **14**, 8533-8557.
23. J. M. Van Doren, L. R. Watson, P. Davidovits, D. R. Worsnop, M. S. Zahniser and C. E. Kolb, *J. Phys. Chem.*, 1990, **94**, 3265-3269.
24. J. L. Ponche, C. George and P. Mirabel, *J. Atmos. Chem.*, 1993, **16**, 1-21.
25. M. Schütze and H. Herrmann, *Phys. Chem. Chem. Phys.*, 2002, **4**, 60-67.
26. S. S. Brown, W. P. Dube, P. Karamchandani, G. Yarwood, J. Peischl, T. B. Ryerson, J. A. Neuman, J. B. Nowak, J. S. Holloway, R. A. Washenfelder, C. A. Brock, G. J. Frost, M. Trainer, D. D. Parrish, F. C. Fehsenfeld and A. R. Ravishankara, *J. Geophys. Res. Atmos.*, 2012, **117**.
27. T. B. Ryerson, M. P. Buhr, G. J. Frost, P. D. Goldan, J. S. Holloway, G. Hubler, B. T. Jobson, W. C. Kuster, S. A. McKeen, D. D. Parrish, J. M. Roberts, D. T. Sueper, M. Trainer, J. Williams and F. C. Fehsenfeld, *Journal of Geophysical Research-Atmospheres*, 1998, **103**, 22569-22583.
28. P. R. Bevington and D. K. Robinson, *Data reduction and error analysis*, McGraw-Hill, New York, 2003.

29. Z. L. Fleming, *personal communication of diurnal cycles of O₃, NO and NO₂ measured at Weybourne between 17 and 29 September 2002.*
30. Z. L. Fleming, P. S. Monks, A. R. Rickard, B. J. Bandy, N. Brough, T. J. Green, C. E. Reeves and S. A. Penkett, *Atmos. Chem. Phys.*, 2006, **6**, 5415-5433.